WIRELESS COMMUNICATIONS AND MOBILE COMPUTING
Wirel. Commun. Mob. Comput. 2008; **8**:1149–1164
Published online 19 October 2007 in Wiley InterScience
(www.interscience.wiley.com) DOI: 10.1002/wcm.558

A comparative study of STBC transmissions at 2.4 GHz over indoor channels using a 2 × 2 MIMO testbed

David Ramírez[1*,†], Ignacio Santamaría[1], Jesús Pérez[1], Javier Vía[1], José A. García-Naya[2], Tiago M. Fernández-Caramés[2], Héctor J. Pérez-Iglesias[2], Miguel González-López[2], Luis Castedo[2] and José M. Torres-Royo[3]

[1]*Departamento de Ingeniería de Comunicaciones, Universidad de Cantabria, 39005 Santander, Spain*
[2]*Departamento de Electrónica y Sistemas, Universidad de A Coruña, 15071 A Coruña, Spain*
[3]*IMS System Engineering, Motorola, Inc., 28027 Madrid, Spain*

Summary

In this paper we employ a 2 × 2 Multiple-Input Multiple-Output (MIMO) hardware platform to evaluate, in realistic indoor scenarios, the performance of different space-time block coded (STBC) transmissions at 2.4 GHz. In particular, we focus on the Alamouti orthogonal scheme considering two types of channel state information (CSI) estimation: a conventional pilot-aided supervised technique and a recently proposed blind method based on second-order statistics (SOS). For comparison purposes, we also evaluate the performance of a Differential (non-coherent) space-time block coding (DSTBC). DSTBC schemes have the advantage of not requiring CSI estimation but they incur in a 3 dB loss in performance. The hardware MIMO platform is based on high-performance signal acquisition and generation boards, each one equipped with a 1 GB memory module that allows the transmission of extremely large data frames. Upconversion to RF is performed by two RF vector signal generators whereas downconversion is carried out with two custom circuits designed from commercial components. All the baseband signal processing is implemented off-line in MATLAB®, making the MIMO testbed very flexible and easily reconfigurable. Using this platform we compare the performance of the described methods in line-of-sight (LOS) and non-line-of-sight (NLOS) indoor scenarios. Copyright © 2007 John Wiley & Sons, Ltd.

KEY WORDS: Multiple-Input Multiple-Output (MIMO); space-time block codes; Blind Channel Estimation; principal component analysis (PCA); MIMO testbeds

1. Introduction

Since the pioneering work of Foschini and Telatar [1,2], multiple transmit and receive antennas have been used to drastically improve the performance of wireless communication systems [3–6]. Specifically, since the work of Alamouti [7], and the later generalization by Tarokh *et al.* [8], space-time block coding (STBC) has emerged as one of the most promising techniques to exploit spatial diversity in Multiple-Input Multiple-Output (MIMO) systems.

Among space-time coding schemes, orthogonal space-time block coding (OSTBC) is one of the most attractive because it is able to provide full diversity gain

*Correspondence to: David Ramírez, Dpt. de Ingeniería de Comunicaciones, Universidad de Cantabria, 39005 Santander, Spain.
[†]E-mail: RamirezGD@gtas.dicom.unican.es

without any channel state information (CSI) knowledge at transmission and with very simple encoding and decoding procedures. The special structure of OSTBCs implies that the optimal maximum likelihood (ML) decoder is a simple linear receiver, which can be seen as a matched filter (MF) followed by a symbol-by-symbol detector. This linear receiver also maximizes the signal-to-noise ratio (SNR) for each data symbol [9] using the knowledge of the channel matrix.

The CSI required for coherent detection of OSTBCs is typically acquired by sending a training sequence that is known at the receiver side [10]. However, the price to be paid is reduced bandwidth efficiency and energy loss because training sequences do not carry information. Popular approaches to avoid these limitations include the so-called Differential STBC (DSTBC) schemes [11–13] and Unitary Space-Time Modulation [14,15], which do not require channel knowledge at the receiver. However, these approaches incur a penalty in performance of 3 dB (differential coding) and 2–4 dB (unitary modulation) as compared to the coherent ML receiver [14]. Moreover, the receiver complexity for the unitary scheme increases exponentially with the number of points in the unitary space-time constellation.

In order to overcome the limitations of differential codes while, at the same time, avoiding the bandwidth reduction of pilot-aided techniques, several methods for blind channel estimation have recently been proposed [16,17]. These methods can be divided into two groups depending on whether they exploit the higher-order statistics (HOS) or the second-order statistics (SOS) of the signals. HOS-based methods exhibit two major drawbacks: they present, in general, a higher computational cost and may require long streams of data to achieve accurate estimates. For these reasons, SOS-based methods are preferable in practice. Recently, a reduced-complexity SOS-based method for blind channel estimation under OSTBC transmissions has been proposed in [18]. Its performance has been evaluated by means of numerical examples, finding that in most cases it renders accurate channel estimates, provided that $n_R > 1$ receive antennas are available. However, for some OSTBCs (including Alamouti) some ambiguities appear that have to be avoided using, for instance, linear precoding at the transmitter or resorting to HOS.

In this paper, we focus on the evaluation of several of the above STBC transmission techniques over realistic indoor scenarios. To this end, we make use of a 2×2 MIMO testbed designed to operate at the 2.4 GHz Industrial, Scientific and Medical (ISM) band. Due to the limitations in the number of transmit antennas, we are constrained to the Alamouti code [7] and the DSTBC for two transmit antennas [11]. For Alamouti coherent decoding, we have employed a pilot-aided CSI estimation technique [10] and the blind technique proposed in [19], which avoids the indeterminacy problems of [18] by reducing in a few bits per second the transmission rate.

The organization of this paper is as follows. In Section 2 the data model for STBC MIMO systems is introduced. Section 3 particularizes this model to OSTBC transmissions and describes the trained and blind channel estimation methods used for coherent detection. In Section 4 we review the encoding and decoding of non-coherent DSTBCs. Section 5 presents the 2×2 MIMO platform used to carry out the measurements. Section 6 compares the utilized MIMO platform with existing testbeds. Section 7 describes the experimental results and presents a comparative study of the different STBC transmission schemes. Finally, the main conclusions are summarized in Section 8.

1.1. Notation

In this paper we will use bold-faced upper case letters to denote matrices, for example, $\mathbf{X}$, with elements $x_{i,j}$; bold-faced lower case letters for column vectors, for example, $\mathbf{x}$, and light-face lower case letters for scalar quantities. The superscripts $(\cdot)^{\mathrm{T}}$ and $(\cdot)^{\mathrm{H}}$ denote transpose and Hermitian, respectively. The real and imaginary parts of a complex quantity will be denoted as $\Re(\cdot)$ and $\Im(\cdot)$, and superscript $\hat{(\cdot)}$ will denote estimated matrices, vectors or scalars. The trace, range (or column space), and Frobenius norm of matrix $\mathbf{A}$ will be denoted as $\mathrm{Tr}(\mathbf{A})$, $\mathrm{range}(\mathbf{A})$, and $\|\mathbf{A}\|$, respectively. The notation $\mathbf{A} \in \mathbb{C}^{M \times N}$ and $\mathbf{A} \in \mathbb{R}^{M \times N}$ will be used to denote that $\mathbf{A}$ is a complex or real matrix of dimension $M \times N$. Finally, the identity matrix of dimensions $p \times p$ will be denoted as $\mathbf{I}_p$ (although the subindex will be omitted when confusion is not possible) and $E[\cdot]$ will denote the expectation operator.

2. Data Model for MIMO STBC Systems

Throughout this paper, we will assume a flat fading MIMO channel model with n_T transmit and n_R receive antennas. The $n_T \times n_R$ complex channel matrix is

$$\mathbf{H} = \left[\mathbf{h}_1 \cdots \mathbf{h}_{n_R}\right] = \begin{bmatrix} h_{1,1} & \cdots & h_{1,n_R} \\ \vdots & \ddots & \vdots \\ h_{n_T,1} & \cdots & h_{n_T,n_R} \end{bmatrix},$$

DOI: 10.1002/wcm

where $h_{i,j}$ denotes the channel response between the ith transmit and the jth receive antennas, and $\mathbf{h}_j$ contains the channel response associated with the jth receive antenna.

Let us consider a space-time block code transmitting M symbols during L time slots and using n_T antennas at the transmitter site. The transmission rate is defined as $R = M/L$ and the symbols of the nth data block are denoted as $r_k[n], k = 1, \ldots, M$. Depending on whether $r_k[n]$ is complex or real, the number of real symbols, M', transmitted in each block is

$$M' = \begin{cases} M & \text{for real constellations,} \\ 2M & \text{for complex constellations} \end{cases}$$

For a STBC, the nth block of data can be expressed in terms of the transmitted real symbols as

$$\mathbf{S}[n] = \sum_{k=1}^{M'} \mathbf{C}_k s_k[n]$$

where $\mathbf{C}_k \in \mathbb{C}^{L \times n_T}$, $k = 1, \ldots, M'$, are the STBC code matrices, and

$$s_k[n] = \begin{cases} \Re(r_k[n]), & k \leq M, \\ \Im(r_{k-M}[n]), & k > M \end{cases}$$

are real symbols. In the case of real STBCs, the code matrices $\mathbf{C}_k$ and therefore the transmitted matrix $\mathbf{S}[n]$ are real.

The signal at the jth receive antenna is

$$\mathbf{y}_j[n] = \mathbf{S}[n]\mathbf{h}_j + \mathbf{n}_j[n] = \sum_{k=1}^{M'} \mathbf{w}_k(\mathbf{h}_j) s_k[n] + \mathbf{n}_j[n]$$

where $\mathbf{n}_j[n]$ is spatial and temporally white complex noise with variance σ^2 and $\mathbf{w}_k(\mathbf{h}_j)$ represents the combined effect of the STBC and the jth channel, which is given by

$$\mathbf{w}_k(\mathbf{h}_j) = \mathbf{C}_k \mathbf{h}_j,$$

for $k = 1, \ldots, M'$.

Taking into account the isomorphism between complex vectors $\mathbf{w}_k(\mathbf{h}_j)$ and real vectors $\tilde{\mathbf{w}}_k(\mathbf{h}_j) = \left[\Re(\mathbf{w}_k(\mathbf{h}_j))^{\mathrm{T}}, \Im(\mathbf{w}_k(\mathbf{h}_j))^{\mathrm{T}}\right]^{\mathrm{T}}$ we can define the real-valued extended code matrices

$$\tilde{\mathbf{C}}_k = \begin{bmatrix} \Re(\mathbf{C}_k) & -\Im(\mathbf{C}_k) \\ \Im(\mathbf{C}_k) & \Re(\mathbf{C}_k) \end{bmatrix}$$

which imply

$$\tilde{\mathbf{w}}_k(\mathbf{h}_j) = \tilde{\mathbf{C}}_k \tilde{\mathbf{h}}_j \tag{1}$$

with $\tilde{\mathbf{h}}_j = \left[\Re(\mathbf{h}_j)^{\mathrm{T}}, \Im(\mathbf{h}_j)^{\mathrm{T}}\right]^{\mathrm{T}}$.

Defining now the real vectors $\tilde{\mathbf{y}}_j[n] = \left[\Re(\mathbf{y}_j[n])^{\mathrm{T}}, \Im(\mathbf{y}_j[n])^{\mathrm{T}}\right]^{\mathrm{T}}$ and $\tilde{\mathbf{n}}_j[n] = \left[\Re(\mathbf{n}_j[n])^{\mathrm{T}}, \Im(\mathbf{n}_j[n])^{\mathrm{T}}\right]^{\mathrm{T}}$, the above equation can be rewritten as

$$\begin{aligned} \tilde{\mathbf{y}}_j[n] &= \sum_{k=1}^{M'} \tilde{\mathbf{w}}_k(\mathbf{h}_j) s_k[n] + \tilde{\mathbf{n}}_j[n] \\ &= \tilde{\mathbf{W}}(\mathbf{h}_j)\mathbf{s}[n] + \tilde{\mathbf{n}}_j[n] \end{aligned}$$

where $\mathbf{s}[n] = [s_1[n], \ldots, s_{M'}[n]]^{\mathrm{T}}$ contains the M' transmitted real symbols and $\tilde{\mathbf{W}}(\mathbf{h}_j) = [\tilde{\mathbf{w}}_1(\mathbf{h}_j) \cdots \tilde{\mathbf{w}}_{M'}(\mathbf{h}_j)]$. Finally, stacking all the received signals into $\tilde{\mathbf{y}}[n] = \left[\tilde{\mathbf{y}}_1^{\mathrm{T}}[n], \ldots, \tilde{\mathbf{y}}_{n_R}^{\mathrm{T}}[n]\right]^{\mathrm{T}}$, we can write

$$\tilde{\mathbf{y}}[n] = \tilde{\mathbf{W}}(\mathbf{H})\mathbf{s}[n] + \tilde{\mathbf{n}}[n]$$

where $\tilde{\mathbf{W}}(\mathbf{H}) = \left[\tilde{\mathbf{W}}^{\mathrm{T}}(\mathbf{h}_1) \cdots \tilde{\mathbf{W}}^{\mathrm{T}}(\mathbf{h}_{n_R})\right]^{\mathrm{T}}$, and $\tilde{\mathbf{n}}[n]$ is defined analogously to $\tilde{\mathbf{y}}[n]$.

When $\mathbf{H}$ is known at the receiver, and assuming a Gaussian distribution for the noise, the coherent ML decoder amounts to minimizing the following criterion [20]

$$\hat{\mathbf{s}}[n] = \underset{\mathbf{s}[n]}{\operatorname{argmin}} \left\| \tilde{\mathbf{y}}[n] - \tilde{\mathbf{W}}(\mathbf{H})\mathbf{s}[n] \right\|^2$$

subject to the constraint that the elements of $\hat{\mathbf{s}}[n]$ belong to a finite set $\mathcal{S}$. This is a NP-hard problem and optimal algorithms to solve it, such as *sphere decoding*, can be computationally expensive [4,21–23].

3. Orthogonal STBCs

In the case of orthogonal STBCs (OSTBCs), the matrix $\tilde{\mathbf{W}}(\mathbf{H})$ satisfies

$$\tilde{\mathbf{W}}^{\mathrm{T}}(\mathbf{H})\tilde{\mathbf{W}}(\mathbf{H}) = \|\mathbf{H}\|^2 \mathbf{I} \tag{2}$$

DOI: 10.1002/wcm

which reduces the complexity of the ML receiver to M' independent, parallel searches to find the closest symbols to the estimated signal

$$\hat{\mathbf{s}}_{\mathrm{ML}}[n] = \frac{\tilde{\mathbf{W}}^{\mathrm{T}}(\mathbf{H})\tilde{\mathbf{y}}[n]}{\|\mathbf{H}\|^2}$$

that is, the OSTBC-MIMO channel response vectors $\tilde{\mathbf{w}}_k(\mathbf{h}_j)$ defined in Equation (1) can be seen as the ML equalizers.

The necessary and sufficient conditions on the code matrices to satisfy Equation (2), for $k = 1, \ldots, M'$, are given by [20]

$$\mathbf{C}_k^{\mathrm{H}}\mathbf{C}_l = \begin{cases} \mathbf{I} & k = l, \\ -\mathbf{C}_l^{\mathrm{H}}\mathbf{C}_k & k \neq l \end{cases} \tag{3}$$

It is straightforward to prove that the above condition must also be satisfied by the real extended code matrices.

$$\tilde{\mathbf{C}}_k^{\mathrm{T}}\tilde{\mathbf{C}}_l = \begin{cases} \mathbf{I} & k = l, \\ -\tilde{\mathbf{C}}_l^{\mathrm{T}}\tilde{\mathbf{C}}_k & k \neq l \end{cases}$$

The most popular OSTBC is the Alamouti code [7], which transmits $M = 2$ complex symbols in $L = 2$ time slots, so the code rate is $R = 1$. The nth block of data for the Alamouti code is

$$\mathbf{S}[n] = \begin{bmatrix} r_1[n] & r_2[n] \\ -r_2^*[n] & r_1^*[n] \end{bmatrix}$$

and the code matrices are

$$C_1 = \begin{bmatrix} 1 & 0 \\ 0 & 1 \end{bmatrix} \quad C_2 = \begin{bmatrix} j & 0 \\ 0 & -j \end{bmatrix}$$
$$C_3 = \begin{bmatrix} 0 & 1 \\ -1 & 0 \end{bmatrix} \quad C_4 = \begin{bmatrix} 0 & j \\ j & 0 \end{bmatrix}$$

In this work we restrict ourselves to the Alamouti code because of the limitation in the number of transmitting antennas of the testbed used in the experiments. The use of a 2×2 platform precludes the use of more sophisticated OSTBCs. Nevertheless, all the current standards using MIMO technologies that are being proposed for different broadband wireless systems, such as IEEE 802.16e (WiMAX) or IEEE 802.20, and evolutions of third generation (3G) systems, such as 3G long-term evolution (LTE), support MIMO systems with two antennas and Alamouti coding for cost and simplicity reasons [24,25].

3.1. Channel Estimation in MIMO-OSTBC Systems

In this section we describe the channel estimation techniques used in the experiments for Alamouti decoding. First, we consider the conventional pilot-based supervised technique and, secondly, we describe a recently proposed blind technique.

3.1.1. Pilot-aided channel estimation

We have applied the channel estimation method described in [10]. Basically, for n_T transmit antennas we need to construct n_T pilot sequences. During the nth frame transmitted from antennas one and two we insert two pilot sequences consisting of K symbols each one

$$\mathbf{S}^{\mathrm{pilot}} = \begin{bmatrix} \mathbf{s}_1^{\mathrm{pilot}} & \mathbf{s}_2^{\mathrm{pilot}} \end{bmatrix} = \begin{bmatrix} s_{1,1} & s_{2,1} & \cdots & s_{K,1} \\ s_{1,2} & s_{2,2} & \cdots & s_{K,2} \end{bmatrix}^{\mathrm{T}}$$

The pilot sequences are designed to be orthogonal

$$\left(\mathbf{s}_i^{\mathrm{pilot}}\right)^{\mathrm{H}} \mathbf{s}_l^{\mathrm{pilot}} \propto \delta_i^l$$

where δ_i^l is the Kronecker delta. This orthogonality among the pilot sequences allows us to estimate independently the fading coefficient from each transmitting antenna to each receiving antenna. Specifically, the least squares (LS) estimate of the channel coefficient between the ith transmit antenna and the jth receive antenna is given by

$$\hat{h}_{i,j} = \frac{\left(\mathbf{s}_i^{\mathrm{pilot}}\right)^{\mathrm{H}} \mathbf{y}_j^{\mathrm{pilot}}}{\left\|\mathbf{s}_i^{\mathrm{pilot}}\right\|^2}$$

where $\mathbf{y}_j^{\mathrm{pilot}}$ is the received signal at the jth antenna when $\mathbf{s}_i^{\mathrm{pilot}}$ has been transmitted.

On the other hand, the transmission of a pilot sequence provokes a reduction in the effective E_b/N_0 or, equivalently, a reduction in the effective transmission rate. For instance, if we transmit N_D data symbols and K pilots during the nth frame, the rate

DOI: 10.1002/wcm

reduction factor associated to this technique is

$$R_{\text{pil}} = \frac{N_D}{N_D + K}$$

3.1.2. SOS-based blind channel estimation

Recently, a new method for blind channel estimation under OSTBC transmissions has been proposed in Reference [18]. It is based only on SOS and it is able to blindly identify the channel (up to a real scalar ambiguity) for most of the existing OSTBCs when the number of receive antennas is $n_R > 1$ [26]. However, some OSTBCs (including the Alamouti code used in this paper) cannot be identified by this method due to an additional ambiguity, which must be eliminated by resorting to other information (e.g., linear precoding, non-white source signal, reduced rate, etc.) [18,19,26,27].

In this section, the method proposed in [18] is first summarized, and then it is particularized for the Alamouti scheme using the method proposed in [19] to avoid the ambiguities.

Let us start by writing the $2n_RL \times 2n_RL$ correlation matrix of $\tilde{\mathbf{y}}[n]$

$$\mathbf{R}_{\tilde{\mathbf{y}}} = E[\tilde{\mathbf{y}}[n]\tilde{\mathbf{y}}^{\mathrm{T}}[n]] = \tilde{\mathbf{W}}(\mathbf{H})\mathbf{R}_s\tilde{\mathbf{W}}^{\mathrm{T}}(\mathbf{H}) + \frac{\sigma^2}{2}\mathbf{I} \tag{4}$$

where $\mathbf{R}_s = E\left[\mathbf{s}[n]\mathbf{s}^{\mathrm{T}}[n]\right]$ is the source correlation matrix.

The method proposed in [18] is the solution to the following optimization problem

$$\hat{\mathbf{H}} = \underset{\mathbf{H}}{\operatorname{argmax}} \operatorname{Tr}\left(\tilde{\mathbf{W}}^{\mathrm{T}}(\mathbf{H})\mathbf{R}_{\tilde{\mathbf{y}}}\tilde{\mathbf{W}}(\mathbf{H})\right), \quad \text{s.t.} \tilde{\mathbf{W}}^{\mathrm{T}}(\mathbf{H})\tilde{\mathbf{W}}(\mathbf{H}) = \mathbf{I} \tag{5}$$

which is given by any channel matrix $\hat{\mathbf{H}}$ with $\|\hat{\mathbf{H}}\| = 1$ satisfying

$$\operatorname{range}(\tilde{\mathbf{W}}(\hat{\mathbf{H}})) = \operatorname{range}(\tilde{\mathbf{W}}(\mathbf{H})) \tag{6}$$

or, equivalently

$$\tilde{\mathbf{W}}(\hat{\mathbf{H}}) = \tilde{\mathbf{W}}(\mathbf{H})\mathbf{Q}$$

where $\mathbf{Q}$ is an orthogonal matrix.

It has been shown [27] that (5) can also be rewritten as the following principal component analysis (PCA) problem

$$\underset{\hat{\mathbf{h}}}{\operatorname{argmax}}\ \hat{\hat{\mathbf{h}}}^{\mathrm{T}}\tilde{\mathbf{Z}}^{\mathrm{T}}\tilde{\mathbf{Z}}\hat{\hat{\mathbf{h}}}, \qquad \text{s.t.} \qquad \|\hat{\hat{\mathbf{h}}}\| = 1, \tag{7}$$

where the data matrix is defined as $\tilde{\mathbf{Z}} = \left[\tilde{\mathbf{Z}}[0]^{\mathrm{T}} \cdots \tilde{\mathbf{Z}}[N-1]^{\mathrm{T}}\right]^{\mathrm{T}}$, $\tilde{\mathbf{Z}}[n]$ is

$$\tilde{\mathbf{Z}}[n] = \begin{bmatrix} \tilde{\mathbf{y}}_1^{\mathrm{T}}[n]\tilde{\mathbf{C}}_1 & \cdots & \tilde{\mathbf{y}}_{n_R}^{\mathrm{T}}[n]\tilde{\mathbf{C}}_1 \\ \vdots & \ddots & \vdots \\ \tilde{\mathbf{y}}_1^{\mathrm{T}}[n]\tilde{\mathbf{C}}_{M'} & \cdots & \tilde{\mathbf{y}}_{n_R}^{\mathrm{T}}[n]\tilde{\mathbf{C}}_{M'} \end{bmatrix}$$

and $\hat{\hat{\mathbf{h}}}$ is defined as follows

$$\hat{\hat{\mathbf{h}}} = \left[\hat{\hat{\mathbf{h}}}_1^{\mathrm{T}}, \ldots, \hat{\hat{\mathbf{h}}}_{n_R}^{\mathrm{T}}\right]^{\mathrm{T}}$$

Once the channel has been obtained, the transmitted signal is estimated as

$$\hat{\mathbf{s}}[n] = \tilde{\mathbf{Z}}[n]\hat{\hat{\mathbf{h}}}$$

As we mentioned previously, for the particular case of Alamouti coding, this technique cannot be applied due to an indeterminacy caused by (6). Basically, this ambiguity appears when there exists an estimated channel $\hat{\mathbf{H}} \neq c\mathbf{H}$ such that its associated equalization matrix $\tilde{\mathbf{W}}(\hat{\mathbf{H}})$ spans the same subspace as $\tilde{\mathbf{W}}(\mathbf{H})$. For the case of the 2×2 MIMO testbed with Alamouti coding used in the experiments, this indeterminacy implies that the largest eigenvalue of $\tilde{\mathbf{Z}}^{\mathrm{T}}\tilde{\mathbf{Z}}$ has a multiplicity of four [18,26]. This means that the true channels $\mathbf{h}_1$ and $\mathbf{h}_2$ associated to the first and second receive antenna, respectively, belong to the subspace spanned by the four eigenvectors associated to the largest eigenvalue of $\tilde{\mathbf{Z}}^{\mathrm{T}}\tilde{\mathbf{Z}}$.

Several attempts have been made to overcome this ambiguity by resorting to some form of precoding of the source signal. In this paper we use a particularly simple method which has been recently proposed in [19]. There it was proved that any OSTBC transmitting an odd number of real symbols (i.e., M' odd) is identifiable regardless of the number of receiving antennas. Therefore, any non-identifiable complex OSTBC can be made identifiable simply by not transmitting one real symbol per OSTBC block. Obviously the transmission rate is reduced, but this rate penalty can be controlled by eliminating only one real symbol

DOI: 10.1002/wcm

per B OSTBC blocks. In this case, the rate reduction factor is

$$R_{\text{blind}} = \frac{BM' - 1}{BM'}$$

which tends to one for $BM' \gg 1$. Finally, for a fixed number of transmitted OSTBC blocks there is a trade-off between the quality of the channel estimate and R_{blind} as a function of B, an issue that has been discussed in [19].

4. DSTBCs

An alternative to blind decoding methods that also avoids the need of CSI estimation is the use of differential schemes. It is well-known, however, that differential modulations suffer a penalty of 3 dB in comparison to coherent detection. In this section we present the specific encoding and decoding of DSTBC for two transmit and two receive antennas [20] that is included in this comparative study. This particular type of DSTBC is restricted to constant modulus signals ($|r_k[n]| = 1$).

In the sequel of this section we briefly review the encoding and decoding rules of the used DSTBC. More details can be found in [20].

4.1. Encoding Algorithm

Let $\mathbf{X}[n]$ be a set of unitary matrices to be transmitted. In DSTBC schemes we transmit the matrices $\mathbf{T}[n]$, which are constructed as follows:

$$\mathbf{T}[n] = \mathbf{X}[n]\mathbf{T}[n-1]$$

with $\mathbf{T}[0] = \mathbf{I}$. A possible design for the matrices $\mathbf{X}[n]$ is using an OSTBC

$$\mathbf{X}[n] = \frac{1}{\sqrt{M}}\mathbf{S}[n]$$

where the normalization factor $1/\sqrt{M}$ is necessary to obtain $\mathbf{X}[n]\mathbf{X}^{\mathrm{H}}[n] = \mathbf{I}$. As we will see later, this particular choice of unitary matrices reduces the computational complexity of the detector.

4.2. Decoding Algorithm

If we transmit $\mathbf{T}[n]$, the received $L \times n_R$ matrix is

$$\begin{aligned}\mathbf{Y}[n] &= \mathbf{T}[n]\mathbf{H} + \mathbf{N}[n] \\ &= \mathbf{X}[n]\mathbf{T}[n-1]\mathbf{H} + \mathbf{N}[n]\end{aligned}$$

where $\mathbf{Y}[n] = \left[\mathbf{y}_1[n] \cdots \mathbf{y}_{n_R}[n]\right]$, and $\mathbf{N}[n]$ is defined analogously. The ML detection of $\mathbf{X}[n]$ from $\mathbf{Y}[n]$ and $\mathbf{Y}[n-1]$ amounts to maximizing the following cost function [20]

$$J(\mathbf{X}[n]) = \Re\left\{\mathrm{Tr}\left\{\mathbf{X}[n]\mathbf{Y}[n-1]\mathbf{Y}^{\mathrm{H}}[n]\right\}\right\} \quad (8)$$

For arbitrary unitary matrices $\mathbf{X}[n]$ this is a computationally expensive problem; however, using OSTBC matrices the detection of each symbol can be decoupled and the cost function (8) to be maximized takes now the form

$$J(s_1[n], \ldots, s_{M'}[n]) = \sum_{k=1}^{M'} \left(\Re\left\{\mathrm{Tr}\left\{\mathbf{C}_k\mathbf{Y}[n-1]\mathbf{Y}^{\mathrm{H}}[n]\right\}\right\} s_k[n]\right)$$

5. Description of the 2 × 2 MIMO Platform

In this section we describe a flexible and easy-to-use 2×2 MIMO testbed, jointly developed at the Universities of Cantabria and A Coruña (Spain). This MIMO testbed is intended for testing and rapid prototyping of MIMO baseband modules. A schematic diagram of the platform is shown in Figure 1 and a picture of the system is shown in Figure 2. Its basic operation is as follows: signal generation, modulation, and space-time coding at transmission are carried out off-line using MATLAB®. The transmitting PC contains a board to generate the analog signals at an IF of 15 MHz. Since this board is equipped with a large (1 GB) and fast memory, the versatility of the platform is extremely high. The upconversion from IF to the carrier RF frequency of 2.385 GHz is performed by two Agilent ESG E4438C signal generators and the signals are then transmitted through two printed dipole antennas.

At the receiver side, two downconverters specifically designed for this platform translate the RF signal to IF. The IF signals are acquired by the receive

DOI: 10.1002/wcm

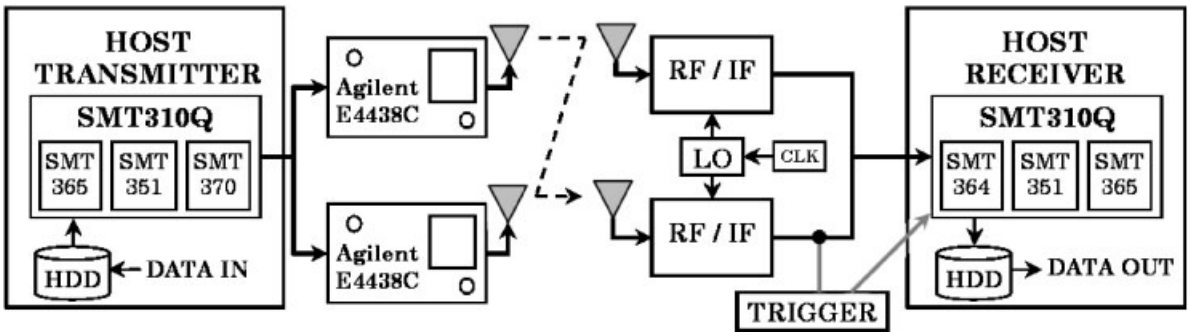

Fig. 1. Schematic diagram of the 2 × 2 MIMO platform.

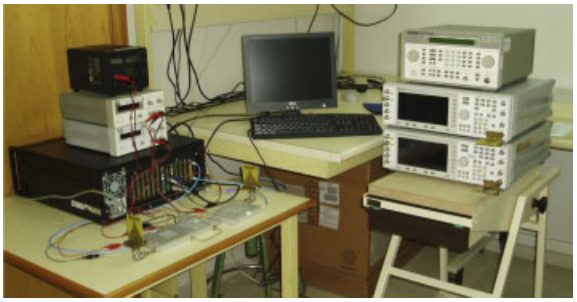

Fig. 2. A picture of the 2 × 2 MIMO platform.

host PC using another board with two ADCs with a maximum sampling frequency of 105 MHz. Another fast and high capacity (1 GB) memory module is used to store the acquired signals. The memory content can be subsequently downloaded into the hard disk of the receiver host PC where synchronization, channel estimation, demodulation, and decoding are performed off-line using MATLAB®.

In the following subsections we present a concise description of the characteristics and capabilities of the baseband and RF subsystems that compose the platform.

5.1. Baseband Modules

5.1.1. Transmitter

The transmitting host (see Figure 3) uses a Sundance SMT310Q PCI carrier board containing the following modules, all compliant with the Texas Instruments Module (TIM) standard : an SMT365 DSP module equipped with the DSP TMS320C6416 from Texas Instruments, 16 MB of ZBTRAM (Zero Bus Turnaround RAM), and a Xilinx Virtex–II XC2V1000

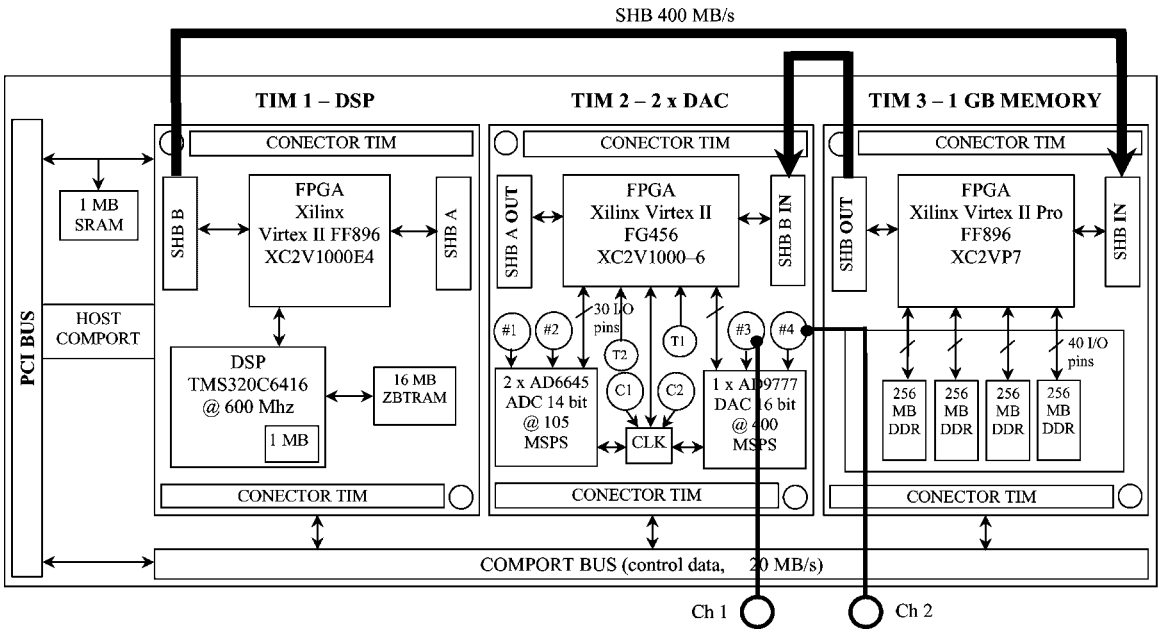

Fig. 3. Schematic diagram of the two antennas baseband transmitter.

DOI: 10.1002/wcm

FPGA; an SMT351 module with 1 GB of DDR SDRAM FIFO memory and an SMT370 DAQ module equipped with one AD9777 dual DAC from Analog Devices. Data transmission among these modules is done through a Sundance High Speed Bus (SHB), working at a clock frequency of 100 MHz and with a total bandwidth of 32 bits, resulting in an overall maximum transfer rate of 400 MB/s. The SHB is divided into two 16-bit wide Sundance Digital Buses (SDB), each of them connected to one of the two transmitting channels. Thus, data are transferred from the memory to the DAC in a multiplexed mode at a maximum speed of 200 MB/s per channel. The transmitting process is controlled by the SMT365 module that contains a DSP at 600 MHz with 1 MB of internal memory. Besides the DSP, this module also contains:

- A Xilinx Virtex-II XC2V1000 FPGA that is used to control the SHB FIFO queue and implements the protocol to control the SHB and the comport buses.
- A 16 MB of ZBTRAM that can be accessed using the EMIF address space at a maximum clock frequency of 133 MHz. This memory is used both as the address space for the DSP application and as a buffer for data transmission. The data set to be transferred through the DAC is read directly from files and stored in the SMT351 memory. During this process, the 16 MB of ZBTRAM are used as a temporary buffer in order to increase the speed of the transfer.
- A Flash ROM of 8 MB that is used to store the FPGA bit stream and the boot code for the DSP.

The SMT365, together with the SMT310Q carrier board, is able to send and receive data from the host using the PCI bus. This feature allows us to transfer large amounts of data at high speeds between the host and the SMT351 module.

The comport bus is used to send the control signals from the SMT365 module to the other modules placed on the SMT310Q carrier board. It achieves 20 MB/s of transfer rate and all the employed modules (i.e., SMT351 and SMT370) are configured by default to read control data from the comport bus.

The SMT351 module is used as a very large FIFO queue for the SHB bus. It is needed because the SMT370 DAC may operate at a clock frequency of 100 MHz and the DSP cannot achieve this speed. So, the data are previously sent to the SMT351 in a cyclic process consisting of reading data from the host and storing it in the SMT351 memory. After reading the data, the transmission starts and the data are transferred from the SMT351 to the SMT370 at the desired speed. This way, the system allows to transfer up to 1 GB of data, which is enough for most scenarios.

The SMT351 module is equipped with a Xilinx Virtex-II Pro FPGA XC2VP7 and 1 GB of double data rate SDRAM at 133 MHz, split in eight memory banks of 256 MB each, that can be accessed in a parallel manner.

Finally, the SMT370 module consists of a Xilinx Virtex-II FPGA and a dual AD9777 DAC from Analog Devices with 16 bits of resolution and a maximum sampling frequency of 400 MHz with interpolation (160 MHz without interpolation). Also, the SMT370 module contains two AD6645 ADCs that are not used by the transmitting host.

The SMT370 has MMBX terminals for the input and the output signal connectors, for clock input and for the trigger signals. Two MMBX wired male BNC connectors are used to transport the signal from/to the SMT370.

The complete configuration is shown in Figure 3 where the SMT365 module is located in TIM 1, the SMT370 in TIM 2 and, finally, the SMT351 in TIM 3. The system requires two comport connections: one to connect the SMT365 to the SMT370 and other to connect the SMT365 with the SMT351. Also, there is an SHB link between the SMT365 and the SMT351 and also between the SMT351 and the SMT370.

In this case the operations of encoding, modulation, and generation of the data files are made off-line in MATLAB®. The data files generated in this way (one per each of the two channels) are read and processed by the DSP application. This program has been developed in C language using the 3L Diamond software which is specially designed to work with the modules and buses previously described. The DSP program also performs:

- The configuration of the transmitter: adjustment of the DAC, initialization of the communication ports, etc.
- The reading of the data files from the host.
- The data transfer, through the SHB, from the DSP to the 1 GB memory module. Later, there data are sent from the memory module to the DAC.

5.1.2. Receiver

The receiving host consists of two devices: an external trigger and a Sundance SMT310Q PCI board which

DOI: 10.1002/wcm

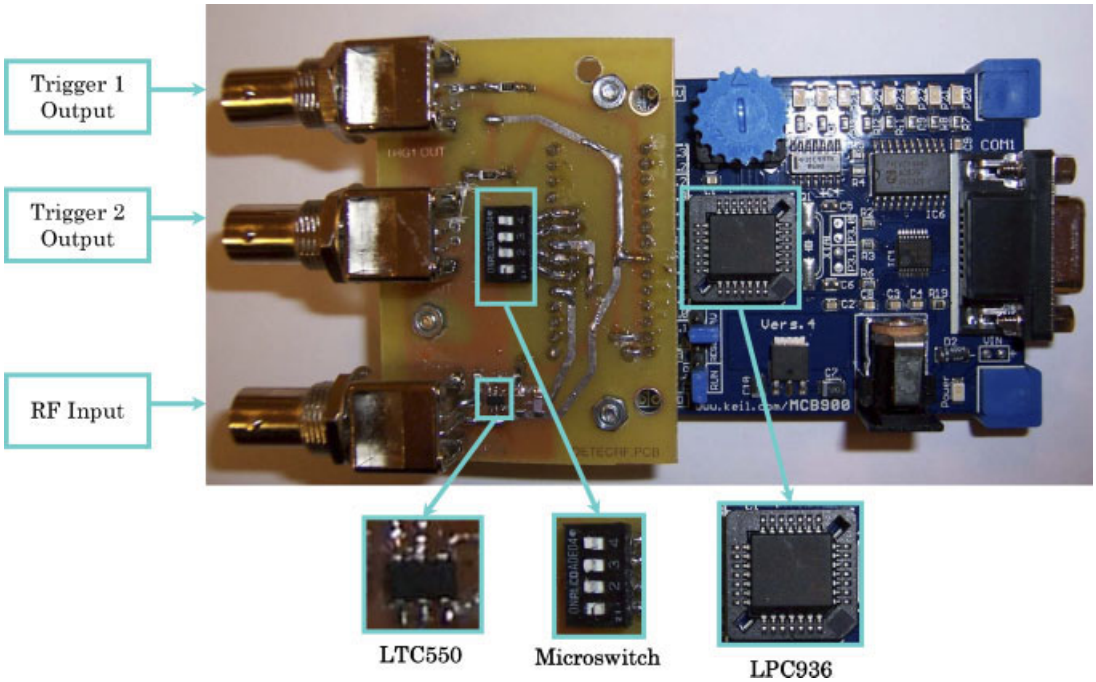

Fig. 4. The trigger.

carries modules with ADCs, DSPs, FPGAs, and a large amount of memory.

A crucial aspect of the acquisition process is the detection of the presence of the transmitted signal at the receiver. This can be done monitorizing by software the received signal. However, this technique has the following drawbacks:

- Large delay between signal detection and acquisition start, so a lot of data are lost.
- Very poor computational efficiency: the involved algorithms are quite heavy and slow.
- Require to adjust the transmission/capture times to compensate the monitorization delays.

To avoid these limitations, we have designed a custom triggering hardware device, whose block diagram is shown in Figure 4. This device monitors the received signal power, waking up the ADCs of the receiving host when the detected power goes beyond a prefixed threshold. This external trigger presents the following advantages:

- Being external, it is independent of the rest of the MIMO platform.
- The delay between signal detection and start of acquisition is limited to a few microseconds (the sampling time of the trigger's ADC plus the time to switch on the outputs).
- The power threshold can be easily chosen by means of the onboard switch.

The external trigger has two main components: a power detector and a microcontroller. For the power detector, we decided on the LTC5507 from Linear Technology. This integrated circuit accepts input signals between 1 KHz and 1 GHz, quantifies the power of the signal, and sends a voltage level to the ADC of the microcontroller.

Also, we chose the Philips LPC936 microcontroller due to its fast ADC and its evaluation board availability, that allowed us to easily embed the microcontroller. This microcontroller monitors the voltage coming from the power detector, activating the ADCs of the receiving host when it exceeds the prefixed threshold. The microcontroller software has been developed in C, with the Keil environment and using the LPC935 and LPC936 libraries.

The hardware of the receiving host is quite similar to the hardware used in the transmitter but instead of DACs, it has ADCs (see Figure 5). It consists of a Sundance SMT310Q PCI board which contains the modules SMT365 (with a DSP, a FPGA, and 16 MB of ZBTRAM), SMT351 (1 GB of memory with a FIFO policy), and SMT364 (with four ADCs). Each ADC is a AD6645 from Analog Devices, with a resolution of 14 bits and a maximum sampling frequency of 105 MHz.

DOI: 10.1002/wcm

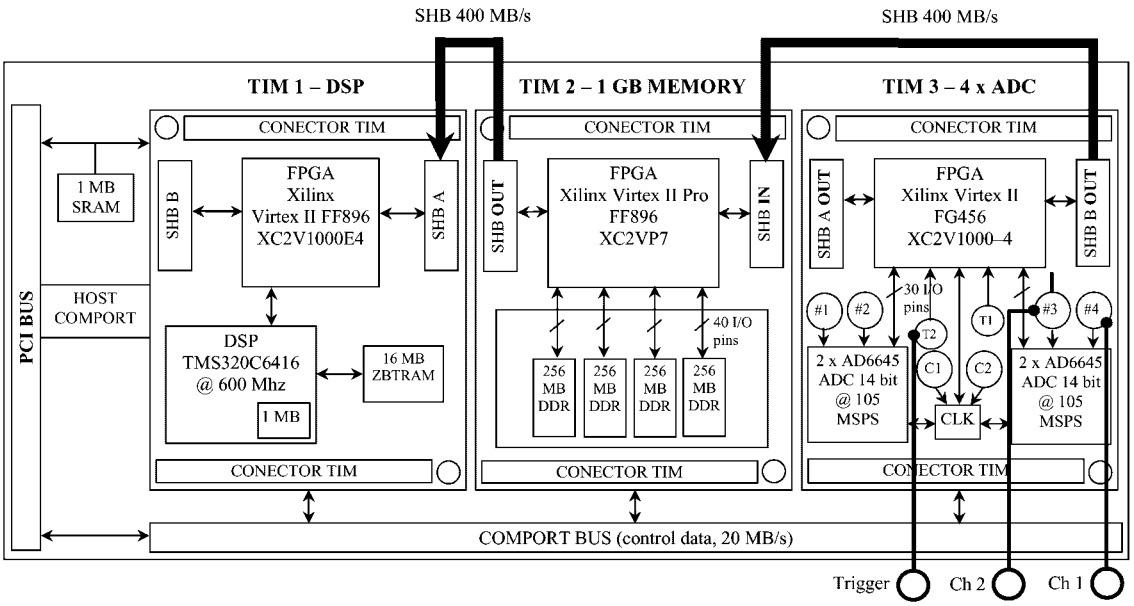

Fig. 5. Baseband RX board.

When the trigger activates the receiving host, the capturing process starts. The signals go through the ADCs and the digital samples are stored in the memory module. When the memory is full, the DSP orders to write the data (or only a part of all the data) to the computer's hard disk. The stored data files can then be processed in MATLAB®.

The software of the receiving host was developed in C using the 3L Diamond API to access to the Sundance hardware. This software performs the following tasks to achieve a right capture:

- Configuration of the receiving host, comprising the initialization of the ADCs, communication ports, the FIFO memory module, etc.
- Writing to the hard disk: the sampled data are read from the memory module and then written in the receiver's hard disk.

Thanks to this flexible scheme, it is really easy to use the MIMO platform with a transmitter and a receiver implemented in MATLAB® or in any other programming language.

5.2. RF Modules

The upconversion from 15 MHz IF to the carrier RF of 2.385 GHz is performed by two Agilent ESG E4438C signal generators. Signals are then radiated by two printed dipole antennas. Let us remark that the signal generators are used merely as upconverters.

At reception, two downconverters translate the RF signal to the IF. The downconverters have been specifically designed for this platform and their main characteristics are the following: bandwidth of 20 MHz (2385 ± 10 MHz), gain of 50 dB, noise figure less than 2 dB, sensitivity of -88 dBm.

6. Testbed Comparison

Different MIMO platforms have been constructed for testing space-time coding and signal processing techniques. Basically, MIMO testbeds can be classified into two main groups. The first one is constituted with those platforms focused on a concrete standard or specification. Examples of this platform type are the narrowband MIMO prototype in [28], the MIMO WCDMA for 3G telephone systems in [29], the MIMO 3G prototype for high-speed downlink packet access reception [30] (both by Lucent Technologies), or the MIMO OFDM testbed for 4G telephone systems by ETRI (Korea) [31]. This type of platforms usually exhibit good technical characteristics but they are extremely expensive and they have poor flexibility capabilities.

On the contrary, our MIMO platform fits into the second type, that is, testbeds designed according to a general purpose. Examples of this type of platforms can be found in [32–42]. To better explain the differences

DOI: 10.1002/wcm

between platforms, we focus on the following features:

- The flexibility of the RF front-ends which allows the platform to be used in different radio frequencies. Our platform is very flexible at transmission because it utilizes commercial signal generators but not at reception where it is limited to a carrier frequency of 2.4 GHz and a bandwidth of 20 MHz. In this sense, our platform outperforms or equals the single-band platforms at 2.4 GHz [33–35,37,38,41,42] but is not capable of receiving signals at higher frequencies and/or higher bandwidths such as [32,36,39,40].
- The characteristics of the memory storage modules at reception and at transmission in terms of capacity and speed which is important for the generation and acquisition of long records of wideband signals. This is one of the most outstanding characteristics of our platform since it has an storage capacity of 512 MB per channel (both at reception and transmission) accessible at the maximum speed of the D/A and A/D converters. This storage capacity is far superior to that of the other platforms.
- The computational power of the processing modules. Our platform has two DSPs with a computational capacity higher than most of the other platforms. Only [34] and [42] are provided with DSPs having similar or superior performance. In terms of FPGA computational capacity, our testbed is only worse than [36] and clearly overcomes [32,35,38,41,42].
- The transfer speed between processing, storage, generation and acquisition units inside the platform. This is a crucial issue for the real-time processing of wideband signals. Our platform together with [35] reaches the highest transfer speed between modules thanks to the utilization of the propietary SHB bus, capable to transfer at the maximum speed of 400 MB/s between modules.

7. Experimental Results

We carried out three different experiments to compare the STBC schemes described in Sections 3 and 4 for two transmit and two receive antennas. More specifically, in this section we present the results obtained for the Alamouti scheme (with pilot-aided channel estimation and with blind channel estimation) and for the DSTBC. Experiments 1 and 2 took place in the laboratory of the Signal Processing Group at the University of Cantabria whereas the third experiment was carried out in the laboratory of the Electronic Technology and Communications Group at the University of A Coruña. In the first experiment the transmitters and the receivers were approximately 2 m away from each other, with a clear line-of-sight (LOS) between them. In the second experiment the transmitters were located farther away from the transmitters ($\approx$10 m) and the transmitting antennas were also moved to avoid a clear LOS (see Figure 6). Finally, in the third experiment, the transmitter and the receivers were approximately 5 m away from each other (see Figure 7). To simplify the symbol and frame synchronization tasks, we designed a frame structure composed of 63 preamble symbols for frame synchronization, up to 64 pilot symbols for channel estimation (for pilot-aided techniques), and 1000 data symbols (see

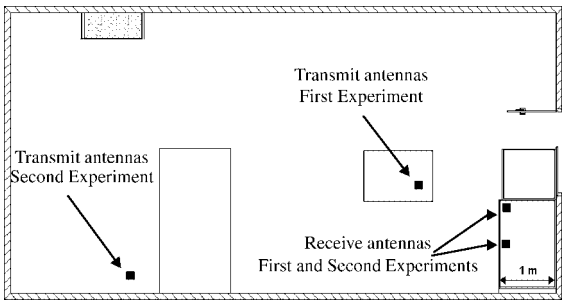

Fig. 6. Antenna locations for the experiments at the University of Cantabria.

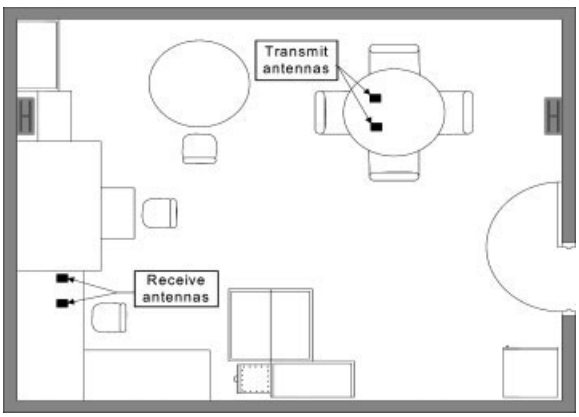

Fig. 7. Antenna locations for the experiment at the University of A Coruña.

DOI: 10.1002/wcm

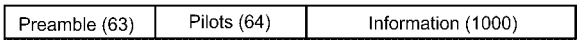

Fig. 8. Frame structure chosen for the experiments.

Figure 8). In the preamble we used a pseudorandom sequence (PN) to facilitate frame synchronization and coarse symbol timing acquisition. Notice that this frame was selected to simplify the synchronization and estimation algorithms and not to maximize throughput.

Regarding the modulation parameters, we employ a QPSK modulation. The pulse shaping filter is a square-root raised cosine filter with a roll-off factor of 0.4. The symbol rate is 1 Mbaud for the first experiment and second experiment and 5 Mbaud for the third experiment, so the RF bandwidth are 1.4 and 7 MHz, respectively. The sampling frequency is 80 Msamples/s at both the transmitter and the receiver. These low symbol rates were used only for illustration purposes, in order to simplify the synchronization and channel estimation algorithms, and to obtain a flat fading channel. There is no problem for the baseband hardware to achieve symbol rates up to 20 Mbaud. At the receiver, we perform carrier offset estimation and eliminate the carrier modulation. Afterwards, frame and symbol synchronization are carried out by exploiting the PN preamble. The final baseband observations are obtained through matched filtering and sampling at the symbol rate.

Now we discuss the results obtained in the first two scenarios (LOS and NLOS at $R_s = 1$ Mbaud.). Figure 9 shows the signal received at one antenna (upper left), the signal after symbol timing (upper right), after carrier frequency offset and symbol timing (lower left), and after Alamouti decoding (lower right). In this example the scenario is LOS and the transmitted power per antenna is -10 dBm.

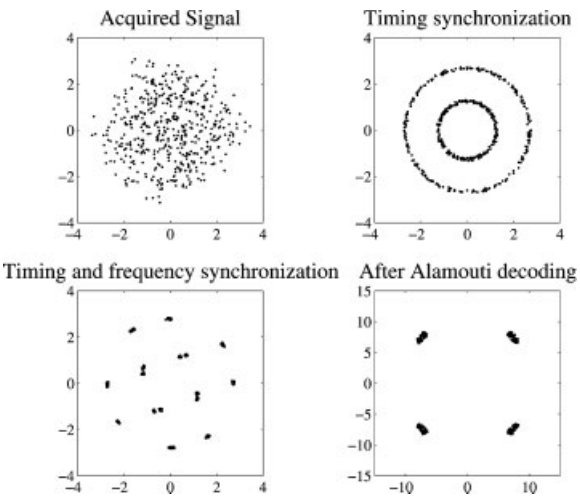

Fig. 9. Symbol constellations at the receiver.

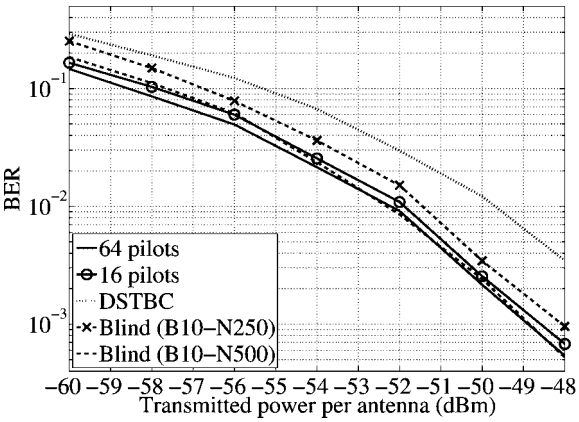

Fig. 10. BER for the LOS experiment.

For both scenarios (LOS and NLOS) we have repeated the experiment varying the transmitting power per antenna and averaging the obtained results. Since the generation and coding at the transmitter side, and the demodulation, channel estimation, and decoding at the receiver side are carried out off-line, the time between two consecutive trials is much larger than the coherence time of the channel and we can assume a block-fading channel. With this setup we obtained the bit error rate (BER) curve *versus* transmitting power, which is shown in Figures 10 and 11 for LOS and NLOS, respectively. Specifically, in these figures we compare:

- The Alamouti scheme with pilot-aided channel estimation (labeled as K pilots).
- The Alamouti scheme with blind channel estimation, labeled as Blind (BX-NY), where X is the number

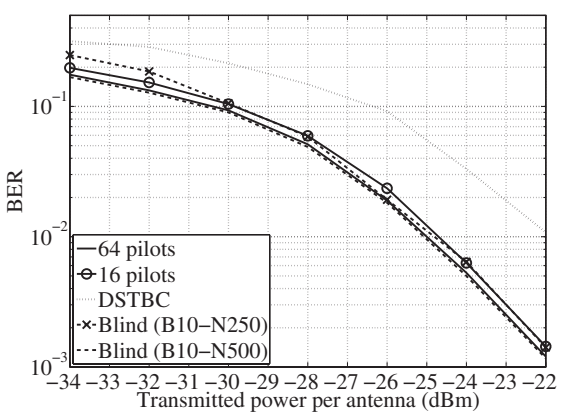

Fig. 11. BER for the NLOS experiment.

DOI: 10.1002/wcm

Table I. Rate for the different channel estimation methods.

Method	Rate
64 pilots	0.9398
16 pilots	0.9843
Blind (B10-N250)	0.9750
Blind (B10-N500)	0.9750

of Alamouti blocks in which we eliminate one real symbol (to avoid the ambiguity) and Y is the number of blocks that we used to estimate the correlation matrix.

- The DSTBC.

It is important to notice that both channel estimation methods (pilot-aided and blind) that we use for coherent detection incur in a rate penalty (see Table I).

As can be seen from Figures 10 and 11, the blind technique with $N = 500$ blocks practically achieves the same performance as the pilot-aided method with 64 pilots. This improvement is achieved at the expense of a moderate increase of the computational cost, since the blind technique has to obtain the main eigenvector of a 8×8 correlation matrix (for this particular setup: Alamouti coding and complex modulation). On the other hand, we also observe the expected 3 dB loss for the DSTBC and that the pilot-aided method with 16 pilots losses about 0.4 dB with respect to the same technique with 64 pilots. We do not employ more than 64 pilots because the channel estimate obtained with more pilots does not improve the performance of the system.

Finally, for the blind technique if we use less blocks for channel estimation, the estimate of the correlation matrix is worst and this causes a loss in BER. Specifically, if we use $N = 250$ instead of $N = 500$ blocks, the loss is about 0.9 dB. However, the use of a reduced number of blocks for blind channel estimation permits the use of shorter frames, which is especially important when the channel coherence time is smaller. These conclusions are valid for both the LOS and NLOS scenarios, the main difference between the two examples is that the NLOS requires an increase of almost 27 dB of transmitting power to attain the same BER.

To gain more insight about the experiments, we have included theoretical references obtained through simulation in Figures 12 and 13. Although we do not have a perfect characterization of the channel, we have found that a Rayleigh and a Rice channel model with a Rice factor of 3 dB are reasonable approximations for the behavior observed in NLOS and LOS scenarios, respectively. Regarding the behavior of the different

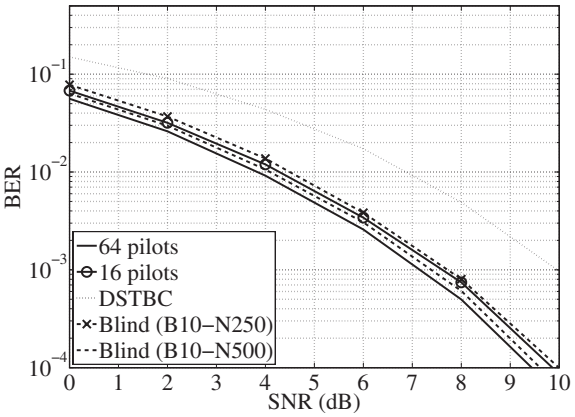

Fig. 12. BER for the Rician simulation.

STBC transmission techniques, the conclusions reached for both the experiments and the simulations are consistent. Despite the similarities there are also some differences between the experimental and the theoretical curves. For instance, the diversity gain estimated as the slope of the BER curve at high SNRs is not the same. This can be attributed to the fact that the actual channel is not exactly Rayleigh (for NLOS) nor Rice (for LOS). Furthermore, the simulations assume uncorrelated channels, but this is not true in practice. Finally, frequency and timing synchronization errors also appear in the experimental curve. A final detail is that for the experimental curves we plot the BER *versus* the transmitted power, whereas for the simulation results we plot the BER *versus* the SNR. The reason for doing this is that for the experimental setup is difficult to have a precise estimate of the SNR at the input of the receiver, since any SNR estimate would also include other impairments such as the channel estimation error, the timming jitter, etc.

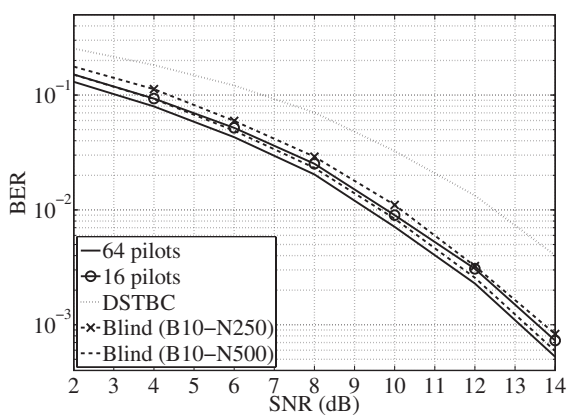

Fig. 13. BER for the Rayleigh simulation.

DOI: 10.1002/wcm

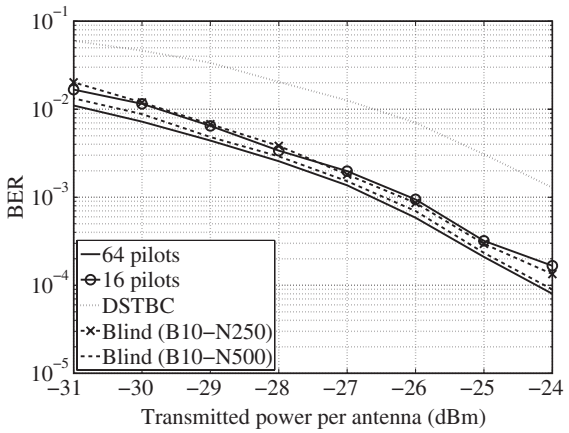

Fig. 14. BER for the 5 Mbaud experiment.

In the third experiment we used a higher transmission rate $R_s = 5$ Mbaud and we obtained the results plotted in Figure 14. These results are very similar to those obtained for experiment 2, as expected since there is not a clear line-of-sight. The results for the third experiment confirm the conclusions obtained for the first and second experiments.

8. Conclusions

In this paper we have compared the performance of several MIMO-STBC systems on real indoor scenarios using a 2×2 MIMO platform at 2.4 GHz. In particular, we have compared the Alamouti orthogonal scheme for two receive antennas with coherent and non-coherent demodulation. We have considered two different channel estimation methods: a conventional pilot-aided technique and a recently proposed blind algorithm based on SOS. We have presented the results obtained from three different experiments. In all cases, the blind channel estimation technique provides similar BER performance than the pilot-aided method, with a slight increase in the effective data rate and a moderate increase in the computational complexity of the detector. On the other hand, the DSTBC presents, as expected, a 3 dB penalty with respect to coherent schemes.

Acknowledgements

This work has been supported by Ministerio de Educación y Ciencia of Spain, Xunta de Galicia and FEDER funds of the European Union under grant numbers TEC2004-06451-C05-02, TEC2004-06451-C05-01, PGIDT05PXIC10502PN, and FPU grants AP2004-5127 and AP2006-2965.

References

1. Foschini G, Gans M. On limits of wireless communications in a fading environment when using multiple antennas. *Wireless Personal Communications* 1998; **6**: 311–335.
2. Telatar IE. Capacity of multi-antenna Gaussian channels. *European Transactions on Telecommunications* 1999; **10**(6): 585–595.
3. Naguib AF, Seshadri N, Calderbank AR. Increasing data rate over wireless channels. *IEEE Signal Processing Magazine* 2000; **17**(3): 76–92.
4. Gesbert D, Shafi M, Shiu D-S, Smith PJ, Naguib A. From theory to practice: an overview of MIMO space-time coded wireless systems. *IEEE Journal on Selected Areas in Communications* 2003; **21**(3): 281–302.
5. Zheng L, Tse D. Diversity and multiplexing: a fundamental tradeoff in multiple-antenna channels. *IEEE Transactions on Information Theory* 2003; **49**(5): 1073–1096.
6. Paulraj AJ, Gore DA, Nabar RU, Bölcskei H. An overview of MIMO communications—a key to gigabit wireless. *Proceedings of the IEEE* 2004; **92**(2): 198–218.
7. Alamouti S. A simple transmit diversity technique for wireless communications. *IEEE Journal on Selected Areas in Communications* 1998; **45**(9): 1451–1458.
8. Tarokh V, Jafarkhani H, Calderbank AR. Space-time block codes from orthogonal designs. *IEEE Transactions on Information Theory* 1999; **45**(5): 1456–1467.
9. Ganesan G, Stoica P. Space-time block codes: a maximum SNR approach. *IEEE Transactions on Information Theory* 2001; **47**(4): 1650–1656.
10. Naguib AF, Tarokh V, Seshadri N, Calderbank AR. A space-time coding modem for high-data-rate wireless communications. *IEEE Journal on Selected Areas in Communications* 1998; **16**(8): 1459–1478.
11. Tarokh V, Jafarkhani H. A differential detection scheme for transmit diversity. *IEEE Journal on Selected Areas in Communications* 2000; **18**(7): 1169–1174.
12. Hughes BL. Differential space-time modulation. *IEEE Transactions on Information Theory* 2000; **46**(7): 2567–2578.
13. Hochwald B, Sweldens W. Differential unitary space-time modulation. *IEEE Transactions on Communications* 2000; **48**(12): 2041–2052.
14. Hochwald B, Marzetta T. Unitary space-time modulation for multiple-antenna communications in rayleigh flat fading. *IEEE Transactions on Information Theory* 2000; **46**(2): 543–564.
15. Hochwald B, Marzetta T, Richardson T, Sweldens W, Urbanke R. Systematic design of unitary space-time constellations. *IEEE Transactions on Information Theory* 2000; **46**(6): 1962–1973.
16. Budianu C, Tong L. Channel estimation for space-time orthogonal block codes. *IEEE Transactions on Signal Processing* 2002; **50**(10): 2515–2528.
17. Stoica P, Ganesan G. Space-time block codes: trained, blind, and semi–blind detection. *Digital Signal Processing* 2003; **13**: 93–105.
18. Shahbazpanahi S, Gershman AB, Manton JH. Closed-form blind MIMO channel estimation for orthogonal space-time block codes. *IEEE Transactions on Signal Processing* 2005; **53**(12): 4506–4517.
19. Vía J, Santamaría I, Pérez J. A sufficient condition for blind identifiability of MIMO-OSTBC channels based on second order statistics. In *Seventh IEEE Workshop on Signal Processing Advances in Wireless Communications*, Cannes, France, July 2006.

DOI: 10.1002/wcm

20. Larsson EG, Stoica P, Ganesan G. *Space-Time Block Coding for Wireless Communications*. Cambridge University Press: New York, U.S.A., 2003.
21. Fincke U, Pohst M. Improved methods for calculating vectors of short length in a lattice, including a complexity analysis. *Mathematics of Computation* 1985; **44**: 463–471.
22. Damen O, Chkeif A, Belfiore J. Lattice code decoder for space-time codes. *IEEE Communications Letters* 2000; **4**(5): 161–163.
23. Jaldén J, Martin C, Ottersten B. Semidefinite programming for detection in linear systems—optimality conditions and space-time decoding. In *IEEE International Conference on Acoustics, Speech, and Signal Processing*, vol. 4, April 2003, pp. 9–12.
24. IEEE 802.16e Std. D12. Air interface for fixed and mobile broadband wireless access system—amendment for physical and medium access control layers for combined fixed and mobile operation in licensed bands. October 2005.
25. Hottinen A, Kuusela M, Hugl K, Zhang J, Raghothaman B. Industrial embrace of smart antennas and MIMO. *IEEE Wireless Communications* 2006; **9**: 8–16.
26. Vía J, Santamaría I. On the blind identifiability of orthogonal space-time block codes from second-order statistics. To appear in *IEEE Transactions on Information Theory*.
27. Vía J, Santamaría I, Pérez J, Ramírez D. Blind decoding of MISO-OSTBC systems based on principal component analysis. In *IEEE International Conference on Acoustic, Speech, and Signal Processing*, Toulouse, France, May 2006.
28. Golden GD, Wolniansky PW, Foschini GJ, Valenzuela RA. V-blast: an architecture for realizing very high data rates over the rich-scattering wireless channel. *Proceedings of International Symposium on Signals, Systems, and Electronics (ISSSE'98)*, pp. 295–300, 1998.
29. Adjoudani A, Beck E, Burg A, *et al*. Prototype experience for MIMO blast over third-generation wireless system. *IEEE Journal on Selected Areas in Communications* 2003; **21**(3): 440–451.
30. Davis L, Knagge G, Garrett G, Woodward G, Nicol C. A 28.8 mb/s 4×4 MIMO 3g high-speed downlink packet access receiver with normalized least mean square equalization. *Proceedings of IEEE International Solid-State Circuits Conference (ISSCC'04)*, vol. 1, pp. 420–536, 2004.
31. Lyu D-S, Won SH, Park HJ. Physical layer implementation and evaluation of multiple input multiple output—orthogonal frequency division multiplexing (MIMO-OFDM) system. *Proceedings of International Conference on Communication Technology (ICCT'03)*, vol. 2, pp. 1348–1352, 2003.
32. Nieto X, Ventura L, Mollfulleda A. Gedomis: a broadband wireless MIMO-OFDM testbed, design and implementation. In *Testbeds and Research Infrastructures for the Development of Networks and Communities, 2006. TRIDENTCOM 2006, 2nd International Conference on*, 2006, pp. 10.
33. Wallace J, Jeffs B, Jensen M. A real-time multiple antenna element testbed for MIMO algorithm development and assessment. In *Antennas and Propagation Society International Symposium, 2004. IEEE*, vol. 2, 2004, pp. 1716–1719 Vol. 2.
34. Mehlfürer C, Maier G, Rupp M, Aschbacher E, Caban S. Design of a flexible and scalable 4×4 MIMO testbed. *11th Digital Signal Processing Workshop*, pp. 178–181, 2004.
35. Langwieser R, Scholtz AL, Caban S, Mehlführer C, Rupp M. Vienna MIMO testbed. *EURASIP Journal on Applied Signal Processing* 2006; **2006**.
36. Borkowski D, Brühl L, Degen C, *et al*. Saba: a testbed for a real-time MIMO system. *EURASIP Journal on Applied Signal Processing* 2006; **2006**. DOI: 10.1155/ASP/2006/54868
37. Morawski R, Le-Ngoc T, Naeem O. Wireless and wireline MIMO testbed. In *Electrical and Computer Engineering, 2003. IEEE CCECE 2003. Canadian Conference on*, vol. 3, 2003, pp. 1913–1916.
38. Murphy P, Lou F, Sabharwal A, Frantz J. An FPGA based rapid prototyping platform for MIMO systems. In *Signals, Systems and Computers, 2003. Conference Record of the Thirty-Seventh Asilomar Conference on*, vol. 1, 2003, pp. 900–904.
39. Guillen i Fàbregas A, Guillaud M, Slock DTM. A MIMO-OFDM testbed for wireless local area networks. *EURASIP Journal on Applied Signal Processing* 2006; **2006**.
40. Lang S, Rao M, Daneshrad B. Design and development of a 5.25 GHz software defined wireless OFDM communication platform. *Communications Magazine, IEEE* 2004; **42**(6): S6–S12.
41. Chiurtu N, Gasser L, Roud P, Rimoldi B. Software-defined radio implementation of multiple antenna systems using low-density parity-check codes. In *Wireless Communications and Networking Conference, 2005 IEEE*, vol. 1, 2005, pp. 527–531.
42. Weijun Zhu MF, Browne D. An open access wideband multi-antenna wireless testbed with remote control capability. *Tridentcom* 2005; 72–81.

Authors' Biographies

David Ramírez received his Telecommunication Engineer Degree from the University of Cantabria, Spain in 2006. Since 2006 he has been pursuing his Ph.D. at the Communications Engineering Department, University of Cantabria, Spain, under the supervision of I. Santamaría. His current research interests include Signal Processing for Wireless Communications, MIMO Systems, MIMO Testbeds and Multivariate Statistical Analysis.

Ignacio Santamaría received his Telecommunication Engineer Degree and his Ph.D. in Electrical Engineering from the Polytechnic University of Madrid, Spain in 1991 and 1995, respectively. In 1992 he joined the Departamento de Ingeniería de Comunicaciones, Universidad de Cantabria, Spain, where he is currently Full Professor. In 2000 and 2004, he spent visiting periods at the Computational NeuroEngineering Laboratory (CNEL), University of Florida. Dr Santamaría has more than 100 publications in refereed journals and international conference papers. His current research interests include Signal Processing Algorithms for Wireless Communication Systems, MIMO Systems, Multivariate Statistical Techniques and Machine Learning Theories. He has been involved in several national and international research projects on these topics.

Jesús Pérez received his M.S. and the Ph.D. in Applied Physics from the University of Cantabria, Spain. In 1989 he joined the Radiocommunication and Signal Processing Department of the Polytechnic University of Madrid, Spain, as a Junior Researcher. From 1990 to 1998, he was at the Electronics Department in the University of Cantabria,

DOI: 10.1002/wcm

first as a Ph.D. student, and later as an Associate Professor. In 1998 he joined the University of Alcalá, Madrid, as an Assistant Professor. From 2000 to 2003 he was with T.T.I. Norte as a Senior Engineer. From 2003 to 2007 he was a Senior Researcher at the Communications Engineering Department in the University of Cantabria, where he is currently an Associate Professor. His main research interests are in the areas of Signal Processing and Information Processing, with a focus on wireless communications.

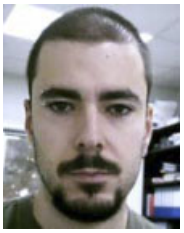

Javier Vía received his Telecommunication Engineer Degree and his Ph.D. in Electrical Engineering from the University of Cantabria, Spain in 2002 and 2007, respectively. In 2002 he joined the Department of Communications Engineering, University of Cantabria, Spain, where he is currently an Assistant Professor. In 2006 he spent a visiting period at the Smart Antennas Research Group (SARG), Stanford University. His current research interests include Blind Channel Estimation and Equalization in Wireless Communication Systems, Multivariate Statistical Analysis and Kernel Methods.

José Antonio García Naya was born in A Coruña, Spain, in 1981. He received the Ingeniero en Informática (M.Sc.) degree in 2005 from Universidade da Coruña, Spain. Since 2005 he is working in the Departamento de Electrónica y Sistemas at Universidade da Coruña where he is a Ph.D. student. His research interests are Space-Time Coding, Blind Source Separation and Hardware Implementation of MIMO systems.

Tiago M. Fernández-Caramés was born in A Coruña, Spain, in 1982. He received his M.Sc. degree in Computer Science Engineering in 2005 from Universidade da Coruña, Spain. Since 2005 he has been working in the Departamento de Electrónica y Sistemas at Universidade da Coruña, where he is currently pursuing his Ph.D. His current research interests include MIMO Systems, Iterative Receivers, Sensor Networks and RFID Technology.

Héctor J. Pérez-Iglesias received his M.S. degree in 2004 from Universidade da Coruña, Spain. From the end of 2004 he is a Ph.D. student at the Departamento de Electrónica y Sistemas of Universidade da Coruña. His research interests are in Channel Estimation, Blind Source Separation, with special focus on MIMO systems and their implementation issues.

Miguel González-López was born in Santiago de Compostela, Spain, in 1977. He received the Ingeniero en Informática and the Ph.D. degrees in 2000 and 2004, respectively, both from Universidade da Coruña, Spain. During 2003 he was a Visitor Scholar under the direction of Prof. Dr Garcia-Frias, at the Electrical and Computer Engineering Department, University of Delaware (U.S.A.). From March to August 2004 he was with the Centro de Estudios e Investigaciones Técnicas de Gipuzkoa (CEIT), San Sebastián, Gipuzkoa, Spain. Since September 2004 he is a Lecturer at Universidade da Coruña. His research interests include the Application of the Turbo Principle to Channel Estimation/Equalization and Coding on Graphs, with special focus on their generalization to MIMO systems and their implementation issues.

Luis Castedo was born in Santiago de Compostela, Spain, in 1966. He received the Ingeniero de Telecomunicación and Doctor Ingeniero de Telecomunicación degrees, both from Universidad Politécnica de Madrid (UPM), Spain, in 1990 and 1993, respectively. From 1990 to 1994 he was a Ph.D. candidate in the Departamento de Señales, Sistemas y Radiocomunicación at the UPM where he worked on applications of array processing to digital communications. His Ph.D. studies were funded by the Spanish Ministerio de Educación y Ciencia through a grant form the FPI program. Between 1991 and 1992 he was a Visiting Scholar at the University of Southern California, Los Angeles, California. From November 1994 to October 2001, he was an Associate Professor in the Departamento de Electrónica y Sistemas at Universidad de A Coruña, Spain, where he is currently a Full Professor. Since 2003 he is also chairman of the Department. His research interests are Signal Processing and Digital Communications with special emphasis on Blind Adaptive Filtering, Estimation/Equalization of MIMO channels, Space-Time Coding and Prototyping of digital communication equipments.

Jose Miguel Torres received his Telecommunication Engineer Degree from the Polytechnic University of Madrid, Spain in 1991. That year he joined Telefonica R&D working there for 9 years in network control and services supply systems projects. In 2000, he moved on to Motorola Spain where he has been leading the System Engineering group based in Madrid going through several technologies: GPRS, UMTS, HSPA, and IMS. He has more than 15 publications and five patents presented to the U.S.A. office. He is currently doing his thesis on MIMO systems for WiMax and LTE in the Telecommunications University of Cantabria. His research interests include Wireless Broadband Communications Systems for 4G.

DOI: 10.1002/wcm